Article

JOURNAL OF
biomaterials
applications

Journal of Biomaterials Applications
2014, Vol. 29(2) 243–253

DOI: 10.1177/0885328214521846
jba.sagepub.com
SAGE

Periodontal ligament versus bone marrow mesenchymal stem cells in combination with Bio-Oss scaffolds for ectopic and in situ bone formation: A comparative study in the rat

Bo-Han Yu[1], Qian Zhou[1] and Zuo-Lin Wang[2]

Abstract

The aim of this study was to compare the osteogenic effects of periodontal ligament stem cells (PDLSCs) versus bone marrow mesenchymal stem cells (BMMSCs) in combination with Bio-Oss scaffolds on subcutaneous and critical-size defects in the immunodeficient rat calvarium. PDLSCs and BMMSCs were obtained from the same canine donor. Twenty-four rats were randomly assigned to one of four experimental groups ($n = 6$ each): group A (no-graft negative control), group B (Bio-Oss positive control), group C (BMMSC/Bio-Oss test group), and group D (PDLSC/Bio-Oss test group). Eight weeks post-transplantation, ectopic and in situ bone regeneration was evaluated by micro-computed tomography (μ-CT), histology, histomorphometry, and immunohistochemistry. The stem cell/Bio-Oss constructs were significantly superior to the controls in terms of their ability to promote osteogenesis ($p < 0.01$), while the PDLSC/Bio-Oss construct tended to be superior to the BMMSC/Bio-Oss construct. Thus, engineered stem cell/Bio-Oss complexes can successfully reconstruct critical-size defects in rats, and PDLSCs and BMMSCs are both suitable as seed cells.

Keywords

Bone regeneration, periodontal ligament stem cell, bone marrow mesenchymal stem cell, Bio-Oss, tissue-engineered bone, comparative study

Introduction

Extensive bone defects are of major clinical importance. These bone defects can result from disease, trauma, and fracture nonunion. They can also occur as a consequence of surgical procedures. Early work indicated that autogenous bone is the "gold standard" for repairing such deficiencies, given its safety and efficacy in grafting modalities. Nonetheless, donor site morbidity, bone resorption, and high operative and hospital costs[1,2] have all led to a search for alternative graft materials,[3] including autografts,[4] allografts,[5] xenografts,[6] and bone-mimetic synthetic materials.[7] However, these graft constituents do not always engender encouraging outcomes because each has its own drawbacks (e.g. infection, rejection, and even poor bone formation).[8,9] As such, recent advances in biotechnology have drawn increasing attention to stem cell-based tissue engineering approaches for bone regeneration.

Many studies indicate that certain postnatal stem cells, including bone marrow mesenchymal stem cells (BMMSCs) and periodontal ligament stem cells (PDLSCs), are capable of self-renewal and osteogenic differentiation in vitro.[10,11] Several investigators also report that tissue-engineered biomaterials composed of stem cells and osteoconductive bone substitutes exhibit good ectopic osteogenic potential in vivo, with a pronounced effect on bone formation in the defect region.[12–14] However, the osteogenic capacity of different tissue-derived stem cells obtained from the same

[1]Department of Stomatology, Tongji University, PR China
[2]Center of Implant Dentistry, Hospital of Stomatology, Tongji University, Shanghai, China

Corresponding author:
Zuo-Lin Wang, Center of Implant Dentistry, Hospital of Stomatology, Tongji University, Shanghai 200092, China.
Email: zuolin@tongji.edu.cn

donor has not been adequately assessed, and no study has carefully evaluated the new bone formation properties of tissue-engineered bone originating from disparate stem cell sources in a nude rat model.

The aim of this study was thus to evaluate the ability of tissue-engineered complexes made up of a commercially available Bio-Oss scaffold (Geistlich, USA) and stem cells obtained from either of two different kinds of mesenchymal tissue to generate new bone in subcutaneous and critical-size defects in the nude rat calvarium. The stem cells were derived from the iliac bone marrow (the source of BMMSCs) or the periodontal ligament (PDL) (the source of PDLSCs). The osteogenic superiority of one stem cell type versus the other was then assessed.

Materials and methods

Animals and experimental groups

One healthy beagle dog (18 months old, 14.5 kg, male) and 24 immunodeficient rats (2 months old, 150 g, male) were supplied by the Laboratory Center of Second Military Medical University of Chinese PLA (No. SCXK-Shanghai 2012-0003). The entire experimental procedure was in accordance with the *Regulations of the Administration of Affairs Concerning Experimental Animals* formulated by the Chinese Ministry of Science and Technology.[15] The animals were housed in temperature-controlled rooms, kept in separate cages, fed a standard diet, given water ad libitum, and allowed free movement during the study. The immunodeficient rats were randomly assigned to one of four experimental groups ($n = 6$ each): group A (no-graft negative control), group B (Bio-Oss positive control), group C (BMMSC/Bio-Oss test group), and group D (PDLSC/Bio-Oss test group). The PDLSCs and BMMSCs were obtained from the same canine donor. Bovine-derived Bio-Oss (granule size, 0.25–1 mm) was chosen as a scaffold because it is a natural bone substitute material, with good similarities to human bone.

Stem cell culture and initial selection

The beagle dog was anesthetized via intravenous injection of sodium pentobarbital (20 mg/kg), and two lower incisors were extracted under sterile conditions. The PDL fragments were gently scraped from the intermediate third of the root, minced into small pieces, and placed into a T25 culture flask (Corning, USA). The bone marrow was aspirated from the iliac crest, washed twice with sterile phosphate buffered saline (PBS), and cultured in a second T25 culture flask. All primary tissues or cells were cultured in α-minimal essential medium (MEM) supplemented with 20% fetal bovine serum (FBS) (Gibco, USA), 2 mM L-glutamine, 100 μM L-ascorbate-2-phosphate, 1 mM sodium pyruvate, 50 U/mL penicillin, and 50 μg/mL streptomycin. The cultures were incubated under standard culture conditions (37°C, 5% CO_2). Three days after seeding, the floating tissues or cells were removed, and the spent medium was replaced with fresh medium. The medium was changed twice per week, and passages were performed when the cells reached 80–90% confluence.

STRO-1 was used as a cell surface marker to sort mononuclear cells in flow cytometry assays. This was done to purify PDLSCs and BMMSCs, and to exclude potential hematopoietic cell contamination. Purified PDLSCs and BMMSCs were employed at the same passage for each in vitro experiment. Next, PDLSCs and BMMSCs with a good growth rate and clone-forming capacity were selected. Cells were inoculated into a six-well plate at a density of 1.0×10^4 cells, cultured for 14 days, fixed with 4% formalin, and reacted with Giemsa stain. Cells were observed under a light microscope, and the numbers of clones (cell clusters with a cell number ≥ 50) were counted.

STRO-1-positive PDLSCs and BMMSCs were treated with osteogenic and adipogenic differentiation media, as previously described.[16,17] The induced cells were stained on day 21 with Alizarin Red S (Sigma, USA) to detect calcium mineral deposits and Oil Red O (Sigma) to detect lipid clusters. A 4-cm^2 area at the center of the well was selected for counting, and the percentage of this area taken up by mineralized nodules or lipid clusters was assessed under a light microscope.

The mRNA expression of scleraxis (SCX), a tendon-specific transcription factor, was also employed to evaluate stem cell differentiation via quantitative polymerase chain reaction (q-PCR) analysis. Total RNA was extracted with TRIzol reagent (Invitrogen, USA), and cDNA was synthesized by using a reverse transcription kit (Takara, Japan) and the primers were listed in Table 1. SCX primer sequences were designed by using Primer Premier 5.0 Software (Premier Biosoft, USA) and then commercially synthesized by Shenggong Biotechnology (China). A "two-step", 40-cycle amplification response procedure was employed, with specifications of 95°C for 120 s, 95°C for 15 s, and 61°C for 40 s. SCX mRNA expression levels in each cell type were normalized to glyceraldehyde 3-phosphate dehydrogenase (GAPDH) mRNA expression levels.

Cell seeding and osteogenic differentiation in vitro

Bio-Oss granules were prepared and sterilized by ^{60}Co irradiation. The granules were preincubated with cell culture medium for 24 h and dried at room temperature

Table 1. Primers used in this study.

Gene	Sequence (5′–3′)	
SCX	F	CGACACATGTCCTCTCCCTG
	R	GAGGTCACCCTTGTCTGTGG
BSP	F	CGATTTCCAGTTCAGAGCAGTAGT
	R	CAGCGTCGGATTCATCTTCAT
Col-I	F	TGGGGCAAGACAGTGATCG
	R	GGAGGGAGTTTACAGGAAGCAG
OCN	F	GCTGTGGCCGCACTCTGC
	R	AGAGTGGGGCTGGCCGCTC
GAPDH	F	AAGGTCGGAGTCAACGGATTT
	R	GGTTCACGCCCATCACAAA

before use. Seven days after osteogenic induction, PDLSCs and BMMSCs were detached from the culture dish and separately seeded onto Bio-Oss in 24-well plates at a density of 2×10^6 cells/mL. Cell seeding was repeated four times at 30 min intervals until saturation was finally achieved. PDLSC/Bio-Oss and BMMSC/Bio-Oss constructs were centrifuged at 1000 r/min for 1 min, followed by the addition of osteogenic medium (1 mL). The medium was changed twice per week. Bio-Oss without stem cells was employed as the positive control.

Cell adhesion and proliferation on the Bio-Oss scaffold were next analyzed by cell counting and the 3-(4,5-dimethylthiazol-2-yl)-2,5-diphenyl tetrazolium bromide (MTT) colorimetric assay, respectively, in addition to scanning electron microscopy (SEM). Briefly, the stem cell/Bio-Oss constructs ($n = 3$) were transferred to fresh 24-well plates at 24 h, 48 h, 72 h, and 96 h after cell seeding. Stem cells that had attached to the Bio-Oss scaffold were removed by trypsinization, and the cells were counted. Alternatively, the stem cell/Bio-Oss constructs ($n = 3$) were transferred to fresh 24-well plates on days 3, 7, and 14, and the MTT assay was carried out by using a commercially available assay kit (KeyGEN Biotech, China). The absorbance value for each well was measured at 490 nm with a microtiter plate reader. On day 14, additional stem cell/Bio-Oss constructs were fixed with 2% glutaraldehyde (Philips, Netherlands) for 2 h and subjected to SEM analysis.

To detect in vitro osteogenic differentiation of PDLSCs or BMMSCs within the Bio-Oss construct, an alkaline phosphatase (ALP) activity assay and q-PCR analysis were performed on days 3, 7, and 14. ALP activity was detected by using a commercially available assay kit (Zhongsheng Beikong Biotechnology and Science Inc., China), and absorbance was measured at 410 nm. Expression levels of the osteogenic differentiation flag markers, bone sialoprotein (BSP), collagen type I (Col-I), and osteocalcin (OCN), were detected by q-PCR as described above, with the primers listed in Table 1. BSP, Col-I, and OCN primer sequences were designed by using Primer Premier 5.0 Software (Premier Biosoft, USA) and then commercially synthesized by Shenggong Biotechnology (China).

Surgical procedures and transplantation

PDLSCs and BMMSCs for the in vivo experiments were obtained from the same canine donor and used at the same passage. The animal model was adapted from Spicer et al.[18] Briefly, after shaving and antiseptic preparation of the operative site, the calvarium was exposed under 4% chloral hydrate anesthesia, and a 4 mm-wide critical-size defect was surgically fashioned by using a round bur (Figure 1). Twenty-four critical-size defects were generated and randomly repaired for each of the four groups (no-graft negative control group A, Bio-Oss positive control group B, BMMSC/Bio-Oss test group C, and PDLSC/Bio-Oss test group D). All defects were covered with Bio-Gide (Geistlich, USA), including the empty (ungrafted) wounds in group A.

In a parallel experiment, Bio-Oss granules (group B), BMMSC/Bio-Oss constructs (group C), or PDLSC/Bio-Oss constructs (group D) were transplanted into the subcutaneous pocket on the dorsal surface of the nude rats. For group A, subcutaneous pockets were prepared but received no graft. The soft tissues were then repositioned and carefully sutured. Postsurgical management involved daily intramuscular injection of antibiotics (Cefazolin Sodium for Injection, 0.5 g, NCPC, China) for 7 days. The sutures were removed at 10 days post-surgery. All rats were routinely fed a standard diet until 8 weeks post-surgery, at which time they were sacrificed.

Sample preparation, micro-computed tomography (μ-CT), and histomorphometric analysis

Eight weeks after surgery, all nude rats were euthanized by an overdose injection of chloral hydrate. Bio-Oss-, BMMSC/Bio-Oss-, and PDLSC/Bio-Oss-containing tissue specimens from the subcutaneous pocket on the dorsal surface were removed and fixed with 10% neutral buffered formalin (pH 7.4). Next, the specimens were placed on a sample holder (68 mm wide) and examined on a μ-CT system (Skyscan 1176, Belgium). Scanning was performed with a resolution of 18 μm in the direction parallel to the coronal aspect of each specimen. Digital micro-radiographic images were acquired at 65 kV and 385 μA.

Due to the different size and shape of each ectopic bone specimen and associated defect, a 4 mm × 1.8 mm area located at the center of the graft was chosen as the

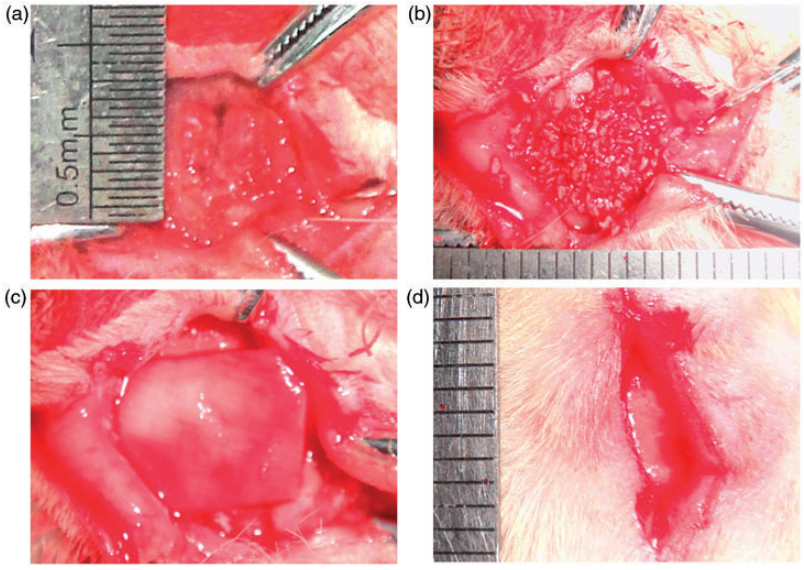

Figure 1. Surgical procedure for the creation of the rat critical-size defect regeneration and ectopic bone formation model. A critical-size defect (4 mm in diameter) was surgically created (a). The surgical defects were then either left alone (negative control group A) or filled with grafts of interest (Bio-Oss scaffold alone (positive control group B), BMMSCs/Bio-Oss construct (group C), or PDLSCs/Bio-Oss construct (group D)) (b). Next, the defects were covered with Bio-Gide (c). Alternatively, grafts B, C, or D were transplanted into the subcutaneous pocket on the dorsal surface of the rat (d). BMMSCs: bone marrow mesenchymal stem cells; PDLSCs: periodontal ligament stem cells.

region of interest (ROI) to unify the calculation and assessment criteria. Cone-Beam CT-reconstruction® A Sasov software (Skyscan) was used to prepare a three-dimensional (3D) reconstruction from the micro-radiographic images. For this reconstruction, the lower and upper threshold values for bone were assumed to be 95 and 255 Hounsfield units, respectively. The data were analyzed and remodeled by using Mimics 9.1 software (Materialise NV, Belgium). Relevant parameters (bone volume ratio (bone volume/total volume), trabecular thickness, trabecular separation, and trabecular number) within the ROI were calculated for each group of rats.

In the same manner, Bio-Oss-, BMMSC/Bio-Oss-, and PDLSC/Bio-Oss-containing tissue specimens for critical-size defect regeneration were observed by μ-CT. A 2 mm × 1.5 mm area located at the center of each graft was chosen as the ROI. The same parameters as described above were calculated to assess the reparative capacity of each Bio-Oss construct.

Next, the specimens were bisected along the coronal plane (left-to-right direction) and separated into two distinct halves. Ground sections were prepared from one of the two halves by sawing and grinding, as described elsewhere,[19] and the new bone formation area was quantitatively measured at low magnification (40×). The counterpart halves were further decalcified in 10% EDTA and routinely processed into 4 μm-thick paraffin-embedded sections, stained with hematoxylin and eosin (H&E), and observed under a light microscope (Nikon, Japan). Immunostaining was also performed with primary antibodies against OCN and cluster of differentiation 31 (CD31) (Abcam, USA) to investigate ossification and vascularization, respectively. The newly formed bone and blood vessels were evaluated histologically and histomorphometrically by three independent observers.

Statistical analysis

All in vitro experiments were performed in triplicate. Quantitative measurements are expressed herein as the mean ± the standard deviation (SD). Unpaired *t*-testing was done to analyze differences between two groups. The histomorphometric data were evaluated by ANOVA, followed by Tukey's post-hoc test. All statistical analyses were conducted with the SPSS 19.0 statistics software package (IBM, USA). Data were considered statistically significant at $p < 0.05$.

Results

Cell culture

STRO-1-positive PDLSCs (Figure 2a1) and BMMSCs (Figure 2b1) both exhibited a typical flat fibroblastic, spindle-like morphology. Notably, PDL-related SCX mRNA was highly expressed in PDLSCs but not in BMMSCs (Figure 2c1), in keeping with the different tissue sources for the two stem cell types. PDLSCs

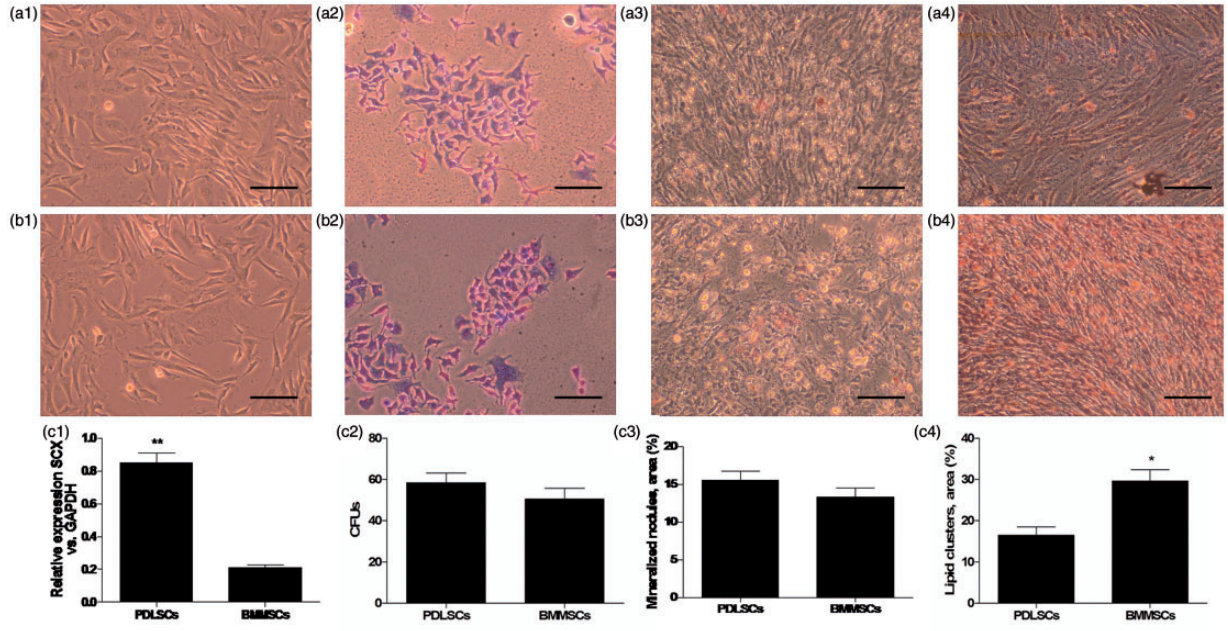

Figure 2. Morphological characteristics, colony-forming capacity, and differentiation potential of PDLSCs and BMMSCs in vitro. STRO-1-positive PDLSCs and BMMSCs showed a spindle-like morphology (a1 and b1, 200×), but PDLSCs expressed higher levels of SCX mRNA than BMMSCs (c1). PDLSCs and BMMSCs were similarly capable of forming colonies (a2 and b2, 200×, c2). Mineralized deposits and lipid clusters were observed for both PDLSCs (a3 and a4, 200×) and BMMSCs (b3 and b4, 200×). However, PDLSCs exhibited a somewhat higher osteogenic potential (c3) and a significantly lower adipogenic potential (c4) than BMMSCs. The high expression of SCX mRNA in PDLSCs vs. BMMSCs (c1) emphasized the different origin of the two stem cell types (*, significantly different vs. PDLSCs ($p < 0.05$); **, significantly different vs. BMMSCs ($p < 0.01$)). Scale bars, 100 μm. BMMSCs: bone marrow mesenchymal stem cells; PDLSCs: periodontal ligament stem cells; SCX: scleraxis.

(Figure 2a2) and BMMSCs (Figure 2b2) both formed individual colonies at 14 days after plating at low density. Nevertheless, no statistically significant differences were observed for colony-forming unit (CFU) behavior between the PDLSCs and BMMSCs (Figure 2c2). After osteogenic and adipogenic induction for 21 days, Alizarin Red S-positive mineralized nodules (Figure 2a3, b3) and Oil Red O-positive lipid clusters (Figure 2a4, b4) were observed in each cell population. However, the size of the Alizarin Red S-positive mineralized nodule area tended to be larger for PDLSCs than for BMMSCs (Figure 2c3). By contrast, Oil Red O staining showed a significantly lower area per well for PDLSCs than for BMMSCs (Figure 2c4, $p < 0.05$). Therefore, all things considered, PDLSCs exhibited a somewhat higher osteogenic potential and a dramatically lower adipogenic potential than BMMSCs.

Adhesion, proliferation, and osteogenic differentiation of stem cells on Bio-Oss

Cell number and proliferation of PDLSCs and BMMSCs on the Bio-Oss granules were assessed at 24, 48, 72, and 96 h after cell seeding. A similar number of PDLSCs and BMMSCs were observed on the scaffolds at 24 h (Figure 3a), indicating comparable levels of initial cell adhesion. The number of total PDLSCs and BMMSCs (Figure 3a), as well as actively proliferating cells (Figure 3b), increased gradually with time, but no clear differences were observed between the two cell populations. In agreement with Figure 2, the stem cells were well-spread on the Bio-Oss scaffold and exhibited a similar spindle-like and flattened appearance in SEM images (PDLSCs, Figure 3c; BMMSCs, Figure 3d), although some of the cells were round. No obvious changes in biocompatibility/morphology were distinguished for either of the two stem cell types under these conditions (Figure 3c, d). Moreover, ALP activity increased over time for both PDLSCs and BMMSCs in the context of the Bio-Oss scaffold, indicating osteogenic differentiation, but neither stem cell type was superior to the other (Figure 3e). The mRNA expression levels of the osteogenic markers BSP, Col-I, and OCN increased during the course of the experiment, with similar trends for PDLSCs and BMMSCs (Figure 3f–h).

General and clinical observations

The surgical procedure was uneventful for all animals. Macroscopically, no visible adverse tissue reactions,

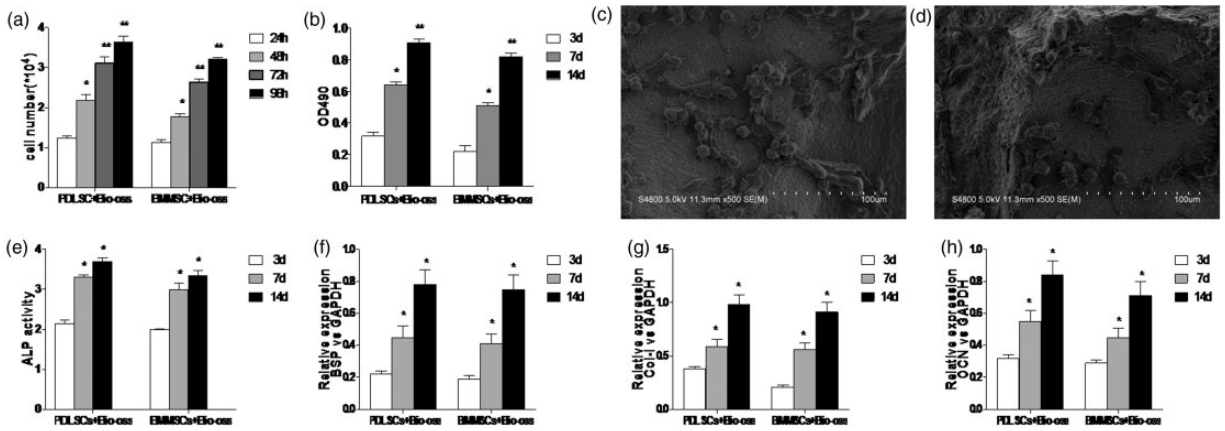

Figure 3. Quantitative assessment of attachment/adhesion, proliferation, and osteogenic differentiation of PDLSCs and BMMSCs on Bio-Oss scaffolds. Cell counting (a) and MTT assays (b) showed that the initial attachment and the number of total and proliferating PDLSCs and BMMSCs on Bio-Oss granules gradually increased with time, with no significant differences between the stem cell types ($p > 0.05$). PDLSCs and BMMSCs were well-spread on the Bio-Oss scaffold, exhibiting a similar mix of round and spindle-like/flattened cells in SEM images (c and d). ALP activity clearly increased with time in PDLSCs and BMMSCs, again with no significant differences between the stem cell types ($p > 0.05$) (e). q-PCR analysis showed a similar trend for BSP, Col-I, and OCN mRNA expression in the presence of osteogenic differentiation cell culture medium (f, g, and h) (*, **, significantly different vs. earliest time point in culture ($p < 0.05$, $p < 0.01$, respectively)). ALP: alkaline phosphatase; BMMSCs: bone marrow mesenchymal stem cells; BSP: bone sialoprotein; Col-I: collagen type I; MTT: 3-(4,5-dimethylthiazol-2-yl)-2,5-diphenyl tetrazolium bromide; OCN: osteocalcin; PDLSCs: periodontal ligament stem cells; q-PCR: quantitative polymerase chain reaction; SEM: scanning electron microscopy.

such as inflammation, infection, or suppuration, were observed during the entire experimental period (data not shown). At the study end point, specimens were retrieved, and no dislocations or adverse effects were observed (data not shown).

Ectopic bone formation

Quantitative evaluation of new ectopic bone formation was performed by μ-CT at 8 weeks post-surgery (Figure 4). No newly formed bone was found in rats in negative control group A, which received a subcutaneous pocket but no transplanted graft (Figure 4a). Bone volume ratio and trabecular thickness, number, and separation were separately calculated for groups A–D, as shown in Figure 4a. The highest values for bone volume ratio (31.4%), trabecular thickness (0.080 mm), and trabecular number (3.91 mm^{-1}) were found in group D (PDLSC/Bio-Oss construct), as was the lowest value for trabecular separation (0.174 mm). These values tended to differ from the corresponding values in group C (BMMSC/Bio-Oss construct) (30.5%, 0.077 mm, 3.88 mm^{-1}, and 0.177 mm, respectively, $p > 0.05$), and were significantly different from those in positive control group B (Bio-Oss alone) (28.5%, 0.073 mm, 3.60 mm^{-1}, and 0.193 mm, $p < 0.01$). A 3D reconstruction of the ROI at the center of each graft (Figure 4b–d) shows remnants of the biodegradable Bio-Oss granules (pink) and newly-formed bone (white) (Figure 4b3, c3, and d3).

Qualitative and quantitative histological evaluations of ectopic bone formation were next performed (Figure 5). No new bone was observed in negative control group A (empty defect) (data not shown). Different degrees of new bone formation were observed in groups B, C, and D (Figure 5a1, a2, and a3, respectively). The osteoblasts in line with the bone trabecula were positively stained in immunohistochemical assays with a primary antibody against OCN for all three groups (Figure 5b1, b2, and b3). However, both the size of the stained area and the intensity of the staining were more pronounced in groups C and D than in group B. CD31-positive blood vessels were also observed in all three groups (Figure 5c1, c2, and c3), whose extent and intensity of the staining paralleled that of OCN-positive osteoblasts. Furthermore, H&E staining (Figure 5d1, d2, and d3) and quantitative analysis (Figure 5d4) of ground sections revealed that the newly formed bone was more extensive in group C (26.9%) and group D (28.0%) than in group B (22.6%). Although the newly formed bone area was distinctly larger in groups C and D versus group B (Figure 5d4, $p < 0.01$), no significant differences were observed between the two stem cell/Bio-Oss constructs ($p > 0.05$), despite slightly higher values in group D.

Critical-size defect regeneration

Analogous to the results for ectopic bone formation, μ-CT showed a similar trend for new bone formation

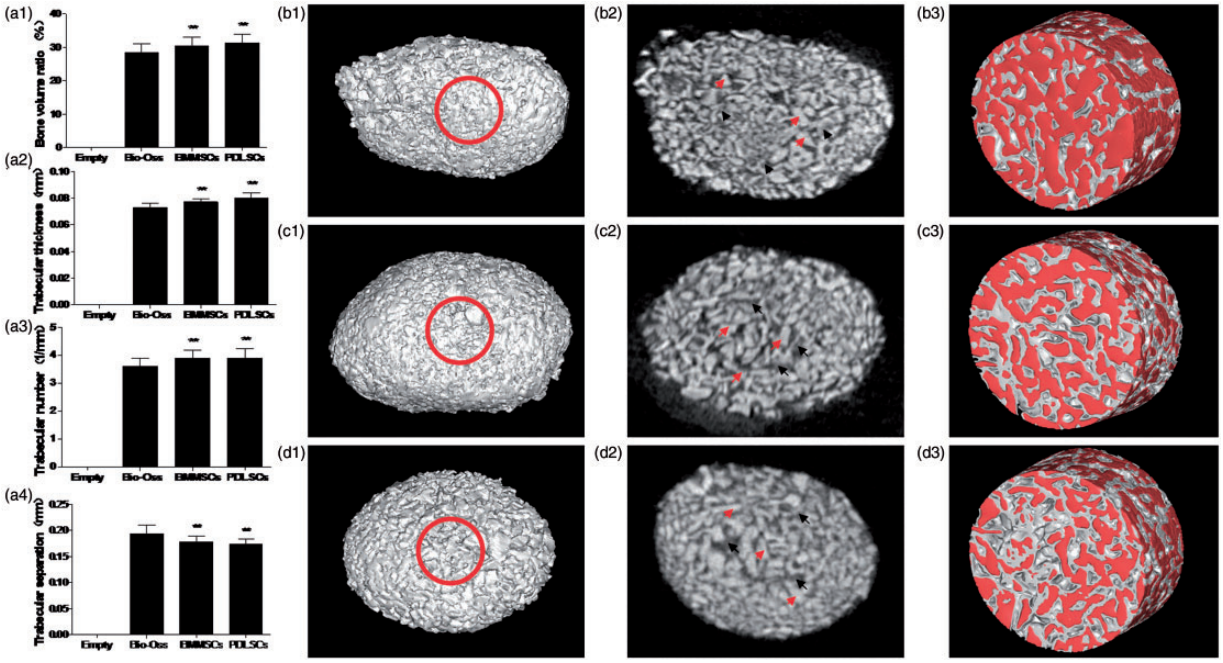

Figure 4. Reconstruction of ectopic bone formation in 3D. Ectopic bone formation was reconstructed in 3D for groups B (Bio-Oss alone), C (BMMSC/Bio-Oss construct), and D (PDLSC/Bio-Oss construct). Data for bone volume ratio, trabecular thickness, trabecular number, and trabecular separation were separately calculated for groups A (negative control (empty)), B, C, and D (a1–a4) (**, significantly different vs. Bio-Oss ($p < 0.01$)). The red circle indicates the ROI for each grafted group (b1, c1, and d1). New bone formation (black arrows) was observed within the Bio-Oss scaffold (red arrows) (b2, c2, and d2). Pink areas represent remnants of the Bio-Oss granules within the 3D-reconstructed image of the ROI in groups B, C, and D (b3, c3, and d3, respectively), and white areas represent newly formed bone. BMMSCs: bone marrow mesenchymal stem cells; PDLSCs: periodontal ligament stem cells; ROI: region of interest.

in the critical-size defect region at 8 weeks post-surgery (Figure 6a, negative control group A (empty defect); 6b, Bio-Oss positive control group B; 6c, BMMSC/Bio-OSS test group C; 6d, PDLSC/Bio-Oss test group D). While a small amount of new bone formation was observed at the edge of the defect in negative control group A, the central region was not repaired (Figure 6a). On the other hand, considerable new bone formation was observed within the Bio-Oss scaffold in group B and particularly in groups C and D (Figure 6b–d). Group D again demonstrated the highest values for bone volume ratio (48.6%), trabecular thickness (0.165 mm), and trabecular number ($5.13\,mm^{-1}$), and the lowest value for trabecular separation (0.154 mm). The corresponding values for group C were 46.9%, 0.145 mm, $4.88\,mm^{-1}$, and 0.158 mm ($p > 0.05$), whereas those for group B were 41.6%, 0.113 mm, $4.45\,mm^{-1}$, and 0.168 mm ($p < 0.01$) (Figure 6e).

Analysis of the ROI in each ground section (Figure 7a) revealed new bone formation within the scaffold in the critical-size defect area in groups B, C, and D (Figure 7b2, b3, and b4, respectively), and especially in the region adjacent to the host bone. New bone formation was not detected in negative control group A (Figure 7b1). The percentage of newly formed bone was higher in groups D and C than in groups B ($p < 0.01$, Figure 7c) and A. As seen for ectopic bone formation, the amount of newly formed bone was statistically similar in groups C and D, even though the values tended to be higher in group D. Because the Bio-Oss constructs were largely destroyed during the course of decalcification, the relevant detection schemes for bone volume ratio and trabecular characteristics were not performed for the critical-size defects.

Discussion

Immunodeficient rats are an important research model for cell transplantation studies, given that experimentation in these animals can minimize graft rejection and interference from inflammation. Ectopic and in situ bone formation are both vital for the evaluation of osteogenesis and the maturation of the bone in response to transplanted stem cells. Therefore, this investigation made use of a nude rat immunodeficient model, with the subcutaneous dorsal surface and the calvarium as the ectopic and in situ host sites, respectively.

Critical-size defects are defined as in situ defects of a size that do not allow spontaneous bone regeneration/healing during the lifetime of the animal.[20] Hence, critical-size defects are well-suited to the judicious

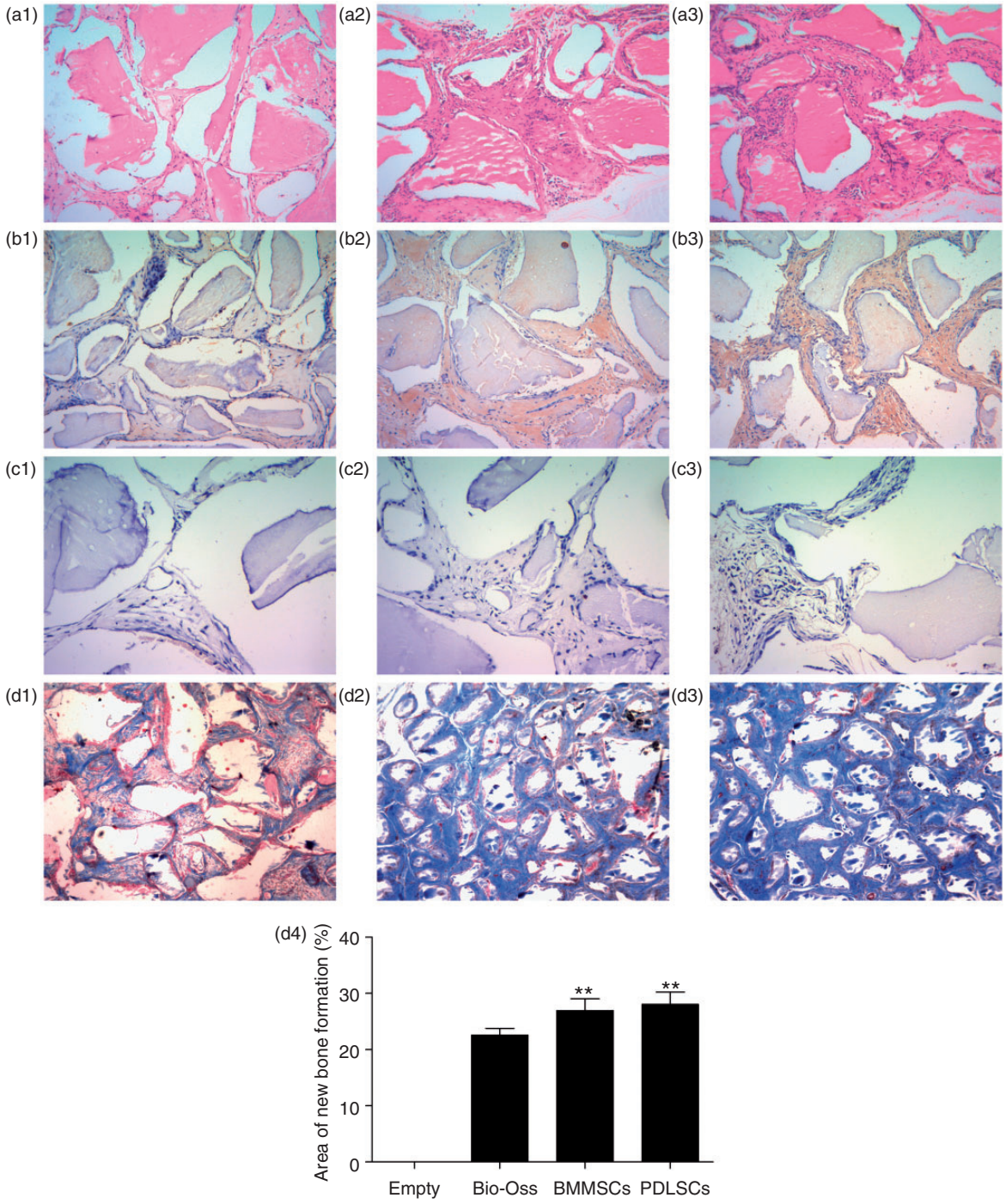

Figure 5. Histological analysis of new ectopic bone formation. Varying degrees of new bone formation were observed. The remnants of the Bio-Oss granules in group B (Bio-Oss scaffold alone, a1, 40×) were larger and more numerous than in groups C and D (a2 and a3, 40×). OCN-positive osteoblasts were detected around the surfaces of the newly formed trabeculae in groups B, C, and D, but the size of the stained area and the intensity of the staining were more pronounced in groups C and D (b2 and b3, 40×) than in group B (b1, 40×). Ground sections also revealed more obvious formation of new vasculature in groups C and D (c2 and c3, 40×) than in group B (c1, 40×). H&E staining is shown in d1–d3, and quantification of the area of new bone formation is shown in d4 (**, significantly different vs. Bio-Oss ($p < 0.01$)). H&E: hematoxylin and eosin; OCN: osteocalcin.

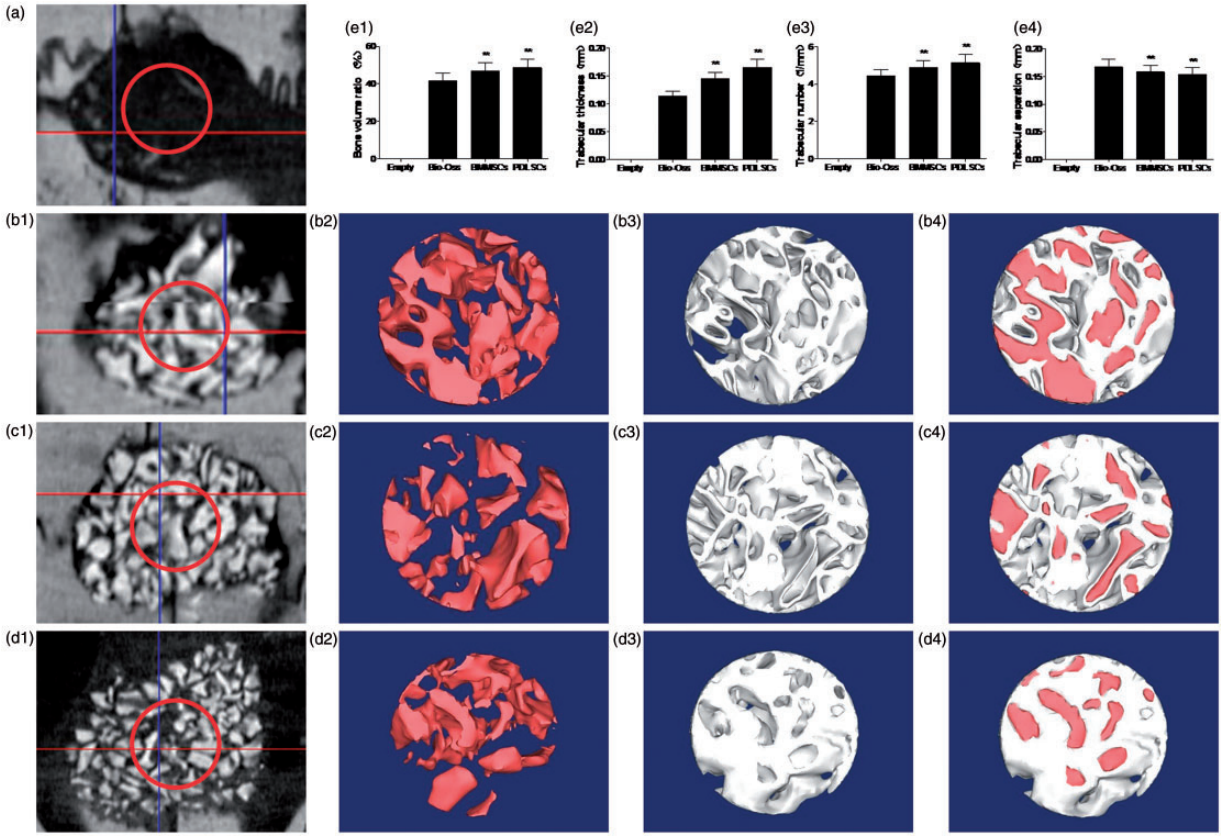

Figure 6. Reconstruction of critical-size defect regeneration in 3D. Critical-size defect regeneration was reconstructed in 3D for groups B, C, and D (Bio-Oss scaffold alone, BMMSC/Bio-Oss, and PDLSC/Bio-Oss, respectively). The red circle indicates the ROI for each grafted group (b1, c1, and d1). A small amount of new bone formation was observed at the edge of the defect in negative control group A (empty defect), but the center region was not yet repaired (a). Pink areas represent remnants of the Bio-Oss granules in groups A, B, and C (b2, c2, and d2, respectively), and white areas represent newly formed bone (b3, c3 and d3) in the 3D-reconstructed image of the ROI (b4, c4, and d4). Data for bone volume ratio, trabecular thickness, trabecular number, and trabecular separation were calculated separately for groups A, B, C, and D (e1–e4) (**, significantly different vs. Bio-Oss ($p < 0.01$)). BMMSCs: bone marrow mesenchymal stem cells; PDLSCs: periodontal ligament stem cells; ROI: region of interest.

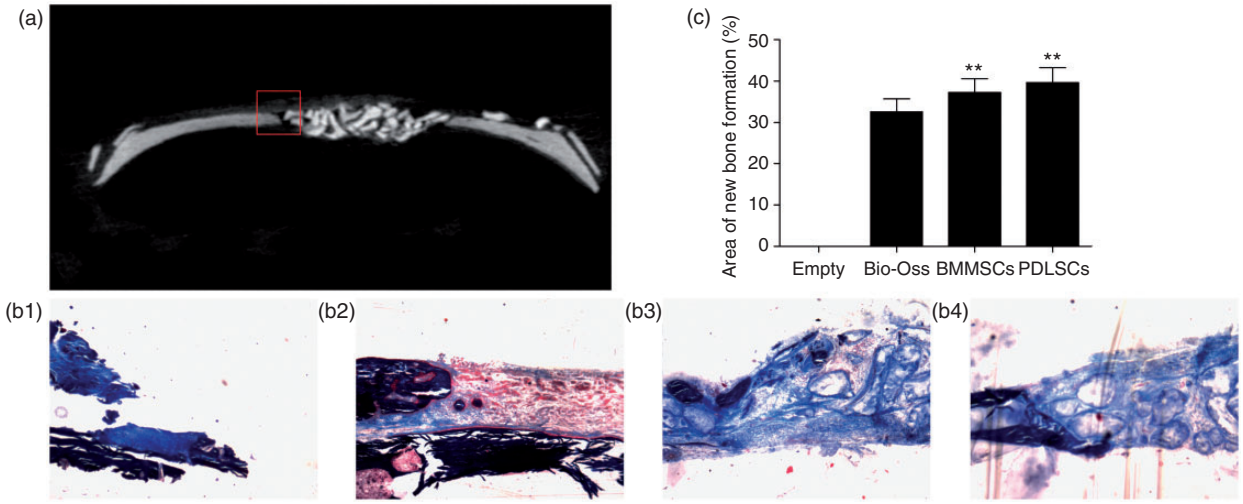

Figure 7. Histological analysis of critical-size defect regeneration. A representative μ-CT image is presented, with the red rectangle indicating the ROI (a). Ground sections (b1–b4, 40×) revealed a more obvious formation of new bone in group C (BMMSC/Bio-Oss, b3) and group D (PDLSC/Bio-Oss, b4) than in group B (Bio-Oss scaffold alone, b2) or group A (empty defect, b1). The area of new bone formation is quantified in (c) (**, significantly different vs. Bio-Oss ($p < 0.01$)). BMMSCs: bone marrow mesenchymal stem cells; μ-CT: micro-computed tomography; PDLSCs: periodontal ligament stem cells; ROI: region of interest.

assessment of tissue-engineered bone because the local environment largely determines the ultimate fate of the transplanted stem cells.[21,22] Along these lines, Bernabé and colleagues[23] demonstrated that the creation of critical-size defects of at least 4 mm in diameter is essential for the careful evaluation of biomaterials in the bone. In the current study, we generated a 4 mm-wide critical-size defect on the calvarium of the nude rat by use of a round bur. No new bone was observed in negative control group A, which received no graft, while different levels of new bone formation were observed in groups B, C, and D, which received Bio-Oss, BMMSC/Bio-Oss, and PDLSC/Bio-Oss constructs, respectively. Thus, the present investigation confirmed the validity of tissue engineering approaches for the repair of critical-size defects in the bone.

The development of tissue engineering techniques has permitted the recent study of various different bone substitutes for bone regeneration. These include autografts (bone harvested from the patient's own body), allografts (bone obtained from a human cadaver or a patient undergoing an operative procedure, such as hip replacement surgery), xenografts (bone obtained from another species, such as the cow), and bone-mimetic synthetic materials (e.g. hydroxyapatite, tricalcium phosphate, and calcium sulfate). However, these materials are all associated with serious drawbacks, including donor-site morbidity and immunological rejection, which has generated interest in stem cell-based transplantation alternatives. The results of the present study, which employed μ-CT, histologic, histomorphometric, and immunohistochemical analyses, provide evidence that Bio-Oss scaffolds seeded with either BMMSCs or PDLSCs are more proficient than unseeded Bio-Oss scaffolds for osteogenesis and new bone formation at 8 weeks post-transplantation. These data unequivocally demonstrate that the addition of stem cells to a bone-mimetic biomaterial can improve the regenerative capacity of tissue-engineered bone.

Selecting the ideal seed cell is integral to the success of any tissue-engineered bone substitute. To this end, we compared the osteogenic effects of BMMSCs and PDLSCs obtained from the same canine donor for ectopic bone tissue engineering and in situ bone regeneration in the nude rat. The PDL-specific protein SCX is a marker for PDL cells or stem cells committed to a PDL fate,[24–26] and q-PCR analysis of SCX mRNA expression successfully distinguished between PDLSCs and BMMSCs in the current study. Our results indicate that PDLSCs represent a unique population of postnatal stem cells that are distinct from BMMSCs.

Although PDLSCs tended to promote superior values than BMMSCs for bone volume ratio and trabecular thickness, number, and separation, both in the subcutaneous pocket and the calvarium, these differences were not statistically significant ($p > 0.05$). It is possible that the differential biological activities of PDLSCs and BMMSCs were affected by the local microenvironment. Notably, PDLSCs are mainly present in the perivascular region, and they can actively differentiate into cementoblast/osteoblast-like cells throughout the lifetime of the organism when faced with appropriate external stimuli.[27] On the other hand, BMMSCs are inclined to differentiate into adipose tissue with aging.[28]

μ-CT is a relatively rapid, precise, and reproducible technique that permits non-destructive imaging and quantitative morphometry of the structure of bone in 3D.[29,30] Various parameters, including bone volume ratio, trabecular thickness, trabecular number, and trabecular separation, are evaluated more precisely by μ-CT than by previously established methods, including planar radiography and medical CT. Furthermore, μ-CT facilitates the collection of vivid images, as shown in Figures 4, 6, and 7. In addition to μ-CT, the current study applied routine analytical measures, ground sections, and morphometry to assess the ossification-promoting effects of the stem cell/Bio-Oss constructs and the amount of newly formed bone. The mRNA expression levels of OCN and CD31, flag markers of ossification and vascularization, were also estimated in ectopic bone formation experiments by immumohistochemical staining. The detection of these markers ensured that the transplanted PDLSCs and BMMSCs encouraged osteogenesis and new blood vessel formation within the tissue-engineered Bio-Oss construct. However, because OCN and CD31 were found in both the stem cell graft and at the host site in the calvarium (data not shown), immunostaining for these markers was abandoned in situ.

In conclusion, the results of the current study demonstrate that stem cell-based, tissue-engineered bone substitutes are promising alternatives to autografts and allografts for the reconstruction of extensive bone defects. Moreover, PDLSCs and BMMSCs were both suitable seed cells for ectopic and in situ bone regeneration in the context of Bio-Oss scaffolds, and the stem cell/Bio-Oss constructs promoted better bone regeneration than Bio-Oss alone. PDLSCs resulted in more osteogenesis than BMMSCs; this may be related to different biological activities of the two stem cell types within the local microenvironment of the transplantation site. Future research in this area will necessitate larger animal models and longer-term observations to confirm the feasibility of stem cell/Bio-Oss constructs for human bone replacement.

Conflict of interest

None declared.

Funding

This study was supported by a research grant (no. 09411955100) from Tongji University to Professor Zuolin Wang, the 2010 Shanghai Committee of Science and Technology of China (grant no. 10XD1404500), and National Natural Science Foundation of China (grant no. 81271110).

References

1. St John TA, Vaccaro AR, Sah AP, et al. Physical and monetary costs associated with autogenous bone graft harvesting. *Am J Orthop (Belle Mead NJ)* 2003; 32: 18–32.
2. Matsa S, Murugan S and Kannadasan K. Evaluation of morbidity associated with iliac crest harvest for alveolar cleft bone grafting. *J Maxillofac Oral Surg* 2012; 11: 91–95.
3. Xu H, Shimizu Y, Asai S, et al. Experimental sinus grafting with the use of deproteinized bone particles of different sizes. *Clin Oral Impl Res* 2003; 14: 548–555.
4. Jensen SS, Broggini N, Weibrich G, et al. Bone regeneration in standardized bone defects with autografts or bone substitutes in combination with platelet concentrate: a histologic and histomorphometric study in the mandibles of minipigs. *Int J Oral Maxillofac Implants* 2005; 20: 703–712.
5. Grover V, Kapoor A, Malhotra R, et al. Bone allografts: a review of safety and efficacy. *Indian J Dent Res* 2011; 22: 496.
6. Accorsi-Mendonça T, Conz MB, Barros TC, et al. Physicochemical characterization of two deproteinized bovine xenografts. *Braz Oral Res* 2008; 22: 5–10.
7. Simunek A, Kopecka D, Somanathan RV, et al. Deproteinized bovine bone versus b-tricalcium phosphate in sinus augmentation surgery: a comparative histologic and histomorphometric study. *Int J Oral Maxillofac Implants* 2008; 23: 935–942.
8. Handschel J, Simonowska M, Naujoks C, et al. A histomorphometric meta-analysis of sinus elevation with various grafting materials. *Head Face Med* 2009; 5: 12.
9. Kim YK, Yun PY, Kim SG, et al. Evaluation of sinus bone resorption and marginal bone loss after sinus bone grafting and implant placement. *Oral Surg Oral Med Oral Pathol Oral Radiol Endod* 2009; 107: e21–e28.
10. Seo BM, Miura M, Gronthos S, et al. Investigation of multipotent postnatal stem cells from human periodontal ligament. *Lancet* 2004; 364: 149–155.
11. Maniat Opoulos C, Sodek J and Melcher AH. Bone formation in vitro by stromal cells obtained from bone marrow of young adult rats. *Cell Tissue Res* 1988; 254: 254–317.
12. Arinzeh TL, Peter SJ, Archambault MP, et al. Allogeneic mesenchymal stem cells regenerate bone in a critical-sized canine segmental defect. *J Bone Joint Surg Am* 2003; 85A: 1927–1935.
13. Nan K, Sun S, Li Y, et al. Ectopic osteogenic ability of calcium phosphate scaffolds cultured with osteoblasts. *J Biomed Mater Res A* 2010; 93: 464–468.
14. Zhu L, Liu W, Cui L, et al. Tissue-engineered bone repair of goat-femur defects with osteogenically induced bone marrow stromal cells. *Tissue Eng* 2006; 12: 423–433.
15. The Ministry of Science and Technology of the People's Republic of China. Regulations for the Administration of Affairs Concerning Experimental Animals 1988-10-31.
16. Mrozik K, Gronthos S, Shi S, et al. A method to isolate, purify, and characterize human periodontal ligament stem cells. *Methods Mol Biol* 2010; 666: 269–284.
17. Park JC, Kim JM, Jung IH, et al. Isolation and characterization of human periodontal ligament (PDL) stem cells (PDLSCs) from the inflamed PDL tissue: in vitro and in vivo evaluations. *J Clin Periodontol* 2011; 38: 721–731.
18. Spicer PP, Kretlow JD, Young S, et al. Evaluation of bone regeneration using the rat critical size calvarial defect. *Nat Protoc* 2012; 7: 1918–1929.
19. Wong FT. An evaluation of various plastic embedding methods for preparing ground sections from calcified tissue with the logitech system for light microscopy. *Calcif Tissue Int* 1985; 37: 669–672.
20. Schmitz JP and Hollinger JO. The critical size defect as an experimental model for craniomandibular nonunions. *Clin Orthop Relat Res* 1986; 205: 299–308.
21. Lin Y, Yan Z, Liu L, et al. Proliferation and pluripotency potential of ectomesenchymal cells derived from first branchial arch. *Cell Prolif* 2006; 39: 79–92.
22. Filip S, Mokrý J, Karbanová J, et al. Local environmental factors determine hematopoietic differentiation of neural stem cells. *Stem cells Dev* 2004; 13: 113–120.
23. Bernabé PF, Melo LG, Cintra LT, et al. Bone healing in critical-size defects treated with either bone graft, membrane, or a combination of both materials: a histological and histometric study in rat tibiae. *Clin Oral Implants Res* 2012; 23: 384–388.
24. Tomokiyo A, Maeda H, Fujii S, et al. Development of a multipotent clonal human periodontal ligament cell line. *Differentiation* 2008; 76: 337–347.
25. Yokoi T, Saito M, Kiyono T, et al. Establishment of immortalized dental follicle cells for generating periodontal ligament in vivo. *Cell Tissue Res* 2007; 327: 301–311.
26. Fujii S, Maeda H, Wada N, et al. Investigating a clonal human periodontal ligament progenitor/stem cell line in vitro and in vivo. *J Cell Physiol* 2008; 215: 743–749.
27. Iwata T, Yamato M and Tsuchioka H. Periodontal regeneration with multi-layered periodontal ligament-derived cell sheets in a canine model. *Biomaterials* 2009; 30: 2716–2723.
28. Nuttall ME and Gimble JM. Is there a therapeutic opportunity to either prevent or treat osteopenic disorders by inhibiting marrow adipogenesis. *Bone* 2000; 27: 177–184.
29. Butz F, Ogawa T, Chang TL, et al. Three-dimensional bone-implant integration profiling using micro-computed tomography. *Int J Oral Maxillofac Implants* 2006; 21: 687–695.
30. Park CH, Abramson ZR, Taba Jr M, et al. Three-dimensional micro-computed tomographic imaging of alveolar bone in experimental bone loss or repair. *J Periodontol* 2007; 78: 273–281.